ACS Catalysis

RESEARCH ARTICLE

pubs.acs.org/acscatalysis

Selective Aerobic Oxidation of Crotyl Alcohol Using AuPd Core-Shell Nanoparticles

Tesfalidet Balcha, Jonathan R. Strobl, Candace Fowler, Priyabrat Dash, and Robert W. J. Scott*

Department of Chemistry, University of Saskatchewan, 110 Science Place, Saskatoon, Saskatchewan, Canada

ABSTRACT: Bimetallic nanoparticles containing Au and Pd were synthesized using poly(vinylpyrrolidone) (PVP) as the polymer stabilizer using both co-reduction and sequential reduction strategies. The nanoparticle structures and catalytic activities for the aerobic oxidation of crotyl alcohol to crotonaldehyde at room temperature in the absence of base were investigated. The chemical, structural, and electronic properties of these nanoparticles were investigated using Pd-K-edge and Au-L_{III}-edge extended X-ray absorption fine structure (EXAFS) spectroscopy and Pd-L_{III} and Au-L_{III} edge X-ray absorption near edge structure (XANES) spectroscopy. EXAFS analysis for the sequentially reduced bimetallic systems indicates the presence of significantly Pd-enriched surfaces and Au cores. XANES spectra of the Pd-L_{III} edges indicated that the sequentially reduced particles showed significant d-charge depletion compared to pure monometallic Pd and co-reduced AuPd nanoparticles. The sequentially reduced nanoparticles with Pd rich surfaces were extremely active for crotyl alcohol oxidation at room temperature in the absence of base, and were quite selective for the formation of crotonaldehyde. A proposed mechanism for the reaction involving the oxidation and re-reduction of Pd on the surface of the particles is postulated based on catalytic activity measurements using sequentially reduced particles and control reactions with Pd^{2+} salts in the absence and presence of Au, Pd, and Pt nanoparticles.

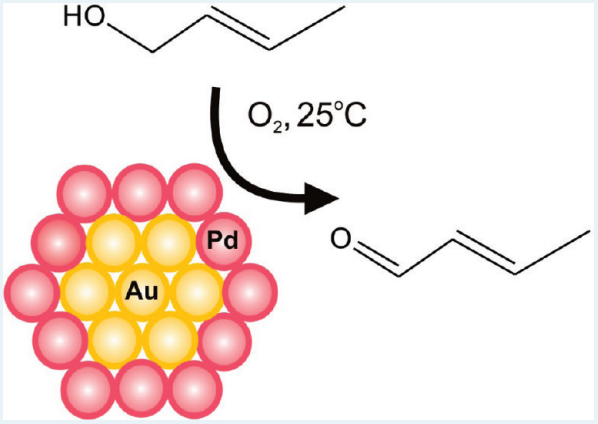

KEYWORDS: quasi-homogeneous catalysis, nanoparticles, alcohol oxidation, structure−property relationships, EXAFS, XANES

INTRODUCTION

The oxidation of alcohols to aldehydes is an essential and widely used organic reaction both in the laboratory scale and in large scale syntheses in industry.[1] Reactions involving the use of homogeneous catalysis for conversion of alcohols to aldehydes are mostly carried out using palladium chloride as a catalyst,[2] or with stoichiometric reagents such as chromates[3] and permanganates.[4] However, such methods produce a large amount of heavy metal waste and are also usually carried out in organic solvents, and are therefore not environmentally benign.[5] To find substitutes for these conventional oxidation catalysts, a lot of development has been made toward the design of new catalysts which can be used in aqueous media and the use of oxygen as an oxidizing agent. However, the use of oxygen under high pressures and temperatures is not desirable because of lack of selectivity, the formation of overoxidation and decomposition products in the reaction mixtures, and explosive hazards associated with the mixing of organic compounds with oxygen under such extreme conditions. Hence many groups are working to develop catalysts which can selectively oxidize alcohols to aldehydes under mild oxygen pressures and temperatures. Recently many groups have shown that monometallic Au,[6−15] Pd,[16,17] and bimetallic AuPd nanoparticles[18−24] can be used as catalysts for aerobic alcohol oxidation under mild conditions in aqueous solutions[8,10,11,20,21] or in solventless conditions.[18,24] Herein we show that sequentially reduced polymer-protected AuPd core-shell nanoparticles are extremely effective catalysts for the selective oxidation of crotyl alcohol to crotonaldehyde in aqueous solutions at room temperature in the absence of base additives.

Earlier studies have shown that Au nanoparticles are quite useful catalysts for low temperature aerobic oxidation reactions. For example, Haruta and co-workers showed that Au nanoparticles are active catalysts for CO oxidation,[25] and both Haruta and Goodman showed that the catalytic activity increases as the mean particle size decreases.[25,26] Tsunoyama and co-workers found that PVP-stabilized Au nanoparticles could be used for the aerobic oxidation of benzyl alcohols in water with high selectivity to aldehyde products.[8,13] Hutchings and others have shown that oxide supported-PdAu nanoparticles are very effective catalysts for the selective oxidation of a wide variety of alcohols in solventless-conditions,[7,18] as well as the oxidation of glycerol,[27,28] and the synthesis of H_2O_2 from H_2 and O_2.[29,30] The improved activity and selectivity for PdAu bimetallic catalysts have been attributed to synergetic effects which originate from electronic and/or geometrical interactions between Au and Pd atoms.[31] Recently we,[20] and others,[21] have demonstrated that PdAu nanoparticles can be used as catalysts for aerobic alcohol oxidation

Received: January 24, 2011
Revised: February 24, 2011
Published: March 10, 2011

in aqueous solutions, and in some cases the reactions can proceed in the absence of base additives.[7,14,15,21] One interesting result in our previous study was the oxidation of the allylic alcohol, crotyl alcohol; initial selectivities of the catalysts toward the formation of crotonaldehyde were quite poor (~40%) but increased dramatically over time.[20] We hypothesized that changes in the internal structure of the PdAu nanoparticles during the catalytic reaction might be responsible for these changes and thus chose to investigate a series of intentionally designed bimetallic structures to see how they behaved as catalysts for this reaction.

Core-shell bimetallic nanoparticles provide a means for the systematic investigation of the electronic properties of catalysts, and also they can minimize the amount of precious metals such as Pt and Pd that are required for catalysis.[32] The synthesis of PdAu bimetallic nanoparticles can be divided into two categories: simultaneous reductions, which involve reduction of both metallic precursors in the same reaction system, and successive reductions which involve the two-step reduction of metallic precursors.[32] We, and others, have previously shown via extended X-ray absorption fine structure (EXAFS) spectroscopy and energy-dispersive spectroscopy (EDS) results that simultaneous reduction of $PdCl_4^{2-}$ and $AuCl_4^-$ salts with a borohydride reducing agent produces near-alloy structures with slightly higher Au concentrations in the core and Pd concentrations on the surface.[33−35] On the other hand both co-reduction and successive reductions of the precursors can yield core-shell,[22,33] cluster-in-cluster structures,[36] alloys,[37] and other structures[38] depending on the reaction conditions and type of reducing agent used. Careful growth of Pd shells onto Au nanoparticle cores (or vice versa) can be done using very mild reducing agents such as ascorbic acid which allow for the minimization of secondary nucleation of new particles while maximizing particle growth to achieve uniform shell thickness.[32,39]

This paper is focused on two points: (1) to synthesize (PVP)-stabilized AuPd nanoparticles via sequential and co-reduction strategies and (2) to completely characterize these catalysts using UV−vis spectroscopy, transmission electron microscopy (TEM), extended X-ray absorption fine structure spectroscopy (EXAFS), and X-ray absorption near edge structure spectroscopy (XANES) to elucidate information on their structure−property relationships. EXAFS and XANES results confirm that the sequential reduction strategy yields particles with approximate core-shell structures with Pd surfaces showing significant d-charge depletion. The AuPd particles were used as catalysts for the selective oxidation of crotyl alcohol to crotonaldehyde at room temperature in the absence of base. Sequentially reduced AuPd nanoparticles were much more selective catalysts for the selective oxidation to crotonaldehyde than their near-alloy or monometallic counterparts. In addition, results show that while Au nanoparticles and K_2PdCl_4 salts each individually show little catalytic activity for crotyl alcohol oxidation at room temperature, together they have significant activity because of the in situ reduction of the Pd salts onto the nanoparticles. Such results provide valuable insights into the possible catalytic mechanisms of AuPd nanoparticles for the oxidation of alcohols.

EXPERIMENTAL SECTION

Materials. Hydrogen tetrachloroaurate (III) hydrate, $HAuCl_4 \cdot 3H_2O$ (99.9%), potassium tetrachloropalladate (II) K_2PdCl_4 (99.99%), poly(vinylpyrrolidone) (PVP) (M.W. 58,000 g/mol), 2-buten-1-ol (97%), *n*-decane (99%), and aluminum isopropoxide (98%) were purchased from Alfa Aesar. Sodium borohydride ($NaBH_4$) (98%), ascorbic acid (99.7%), isopropyl alcohol (99.8%), and nitric acid were purchased from EMD. Ethyl acetate was purchased from Sigma-Aldrich. All these chemicals were used as obtained without any further purification. Dialysis of the nanoparticles was conducted using cellulose dialysis membranes (M_w cutoff 12,400 g/mol) purchased from Aldrich. Eighteen MΩ·cm Milli-Q water (Millipore, Bedford, MA) was used for all nanoparticle syntheses.

Synthesis of Nanoparticles. The preparation of the sequentially reduced nanoparticles was conducted by modifying the general procedure found elsewhere.[32] PVP stabilized Au nanoparticles were made by reducing 1.38 mL of 10.0 mM $HAuCl_4 \cdot 3H_2O$ (1.38×10^{-5} mole) with 1.38 mL of 0.10 M of $NaBH_4$ (1.38×10^{-4} moles) under vigorous stirring in a 1.39 mM PVP solution and followed by the addition of deionized water to give a total volume of 28.50 mL. Then the Au nanoparticles were dialyzed overnight with 1.0 L of deionized water before using them for the sequential synthesis. To prepare sequentially reduced 1:3 AuPd nanoparticles, 10.07 mL of Au nanoparticles (4.80×10^{-6} mol) (Au seeds, concentration refers to [Au]) were mixed with 1.44 mL of 0.10 M ascorbic acid (1.44×10^{-4} mol) followed by the addition of 1.44 mL of 10.0 mM K_2PdCl_4 (1.44×10^{-5} mol), and deionized water to give a total volume of 14.5 mL. The solution was then stirred for 1 h while cooling in an ice bath. Then the nanoparticles were dialyzed overnight to remove excess salts and ascorbic acid before use. The 1:3 AuPd co-reduced nanoparticles were synthesized by simultaneous reduction of 0.48 mL of 10.0 mM (0.48×10^{-5} mol) of $HAuCl_4 \cdot 3H_2O$ and 1.44 mL of 10.0 mM K_2PdCl_4 (1.44×10^{-5} mol) using a ten times excess of sodium borohydride (1.92 mL of 0.10 M $NaBH_4$) as the reducing agent, and deionized water was subsequently added to give a total volume of 14.5 mL.[33] Au, Pd, and other AuPd nanoparticles were prepared following similar procedures while keeping the total molar amount of the metal constant.

Catalytic Measurements. The oxidation of crotyl alcohol was conducted at room temperature (25 °C) using the following procedure. First the previously prepared nanoparticle solution (total moles of metal 1.92×10^{-5} mol) in 14.5 mL solution was purged with oxygen for 5 min. Then 530 μL (1.0×10^{-2} mol) of crotyl alcohol was added to give a substrate/catalyst ratio of 520:1. The products were then extracted by ethyl acetate three times, and decane was added as an internal standard. Conversion, selectivity, and turnover numbers were obtained from GC using a FID detector (Agilent Technologies 7890A) and a HP-Innowax capillary column. At least three catalytic trials were conducted for each catalyst.

Sample Preparation for EXAFS Measurements. Pd, Au, and AuPd co-reduced and core-shell nanoparticles with metal/alumina ratios of 2.5% by weight were synthesized by trapping the as-synthesized particles in alumina following a procedure reported previously.[33] The nanoparticles were dried under vacuum and then redissolved in isopropanol followed by the addition of five drops of a dilute aqueous nitric acid solution (pH ~ 2.0). Then 0.83 g of aluminum isopropoxide dissolved in 15.0 mL of dry isopropanol was added under nitrogen, and the sample was left overnight for gel formation. The gel was then dried under vacuum at 45 °C for 2 h and ground into a fine powder with a mortar and pestle.

Characterization. A Varian Cary50 UV−visible spectrophotometer was used for UV−vis measurements within a scan range of 300−900 nm using a quartz cell with an optical path length of

1.0 cm. A Philips 410 microscope operating at 100 kV was used for TEM imaging. TEM samples were prepared by placing a drop of the solution containing the nanoparticles on a carbon-coated Cu grid which was pretreated by air plasma discharge for 30 s. The Hard X-ray MicroAnalysis beamline (HXMA) 061D-1 (energy range, 5−30 keV; resolution, 1×10^{-4} $\Delta E/E$) at the Canadian Light Source was used for recording X-ray absorption spectra at the Pd K-edge and the Au L_{III}-edge. The beamline optics include water-cooled collimating KB mirrors (Rh for the Au L_{III}-edge and Pt for Pd K-edge), and a liquid nitrogen cooled double crystal monochromator housing two crystal pairs [Si (111) and Si (220)]. The X-ray measurements were conducted in ion chamber filled with a helium and nitrogen mixture for the Au L_{III}-edge and pure helium for the Pd K-edge. The energy scan range for the measurement was between −200 eV to +1000 eV at each edge. Pd and Au foils were used for the respective edges as references. All EXAFS measurements were conducted in transmission mode at room temperature using samples pressed into pellets. Pd-L_{III} XANES spectra were measured using the Soft X-ray Microcharacterization Beamline (SXRMB) 06B1−1 (energy range 1.7−10 keV; resolution, 3.3×10^{-4} to 1×10^{-4} $\Delta E/E$ with InSb(111) and Si(111) crystals) at the Canadian Light Source. Calibration of the Pd-L_{III} spectra was done using the Ar K-edge transition at 3203.54 eV.[40]

The software package IFEFFIT was used for data processing which included fitting the pre-edge region to a straight line, and the background above the edge was fit to a cubic spline function.[41,42] The EXAFS function, χ, was obtained by subtracting the post-edge background from the overall absorption and then normalizing with respect to the edge jump step. The EXAFS fitting was performed in *R*-space between 1.4−3.4 Å for the Au-edge and 1.4−3.0 Å for the Pd-edge using theoretical phase-shifts and amplitudes generated by FEFF. fcc bulk lattice parameters (i.e., first shell coordination numbers of 12) were used to determine the amplitude reduction factor, S_o^2, for Au and Pd by analyzing Au and Pd reference foils and (bis-ethylenediamine)palladium(II) chloride for the Pd−O contribution (Others have also recently used Pd amine complexes to fit Pd−O contributions in PdAu catalysts).[43] The S_0^2 values were found to be 0.84 and 0.88 for Pd and Au, respectively. A homogeneous PdAu alloy model for FEFF fitting was constructed based on bulk PdAu lattice parameters.[44]

RESULTS AND DISCUSSION

The preparation of the bimetallic nanoparticles was conducted following general procedures reported in previous publications.[32,33] PVP was used as the stabilizer partly because of its high solubility in water as well as its ability to provide high stability to the nanoparticles through multiple coordination of the N−C═O groups to the nanoparticle surface.[45] Scheme 1 below shows the stepwise reduction of Pd ions on the surface of preformed gold nanoparticles, and two possible final structures (core-shell and cluster-in-cluster). The mild reducing agent ascorbic acid was used for the reduction of Pd to minimize the degree of secondary nucleation while maximizing the particle growth to achieve a uniform shell thickness. Figure 1 illustrates the UV−vis spectra of Au nanoparticles and sequentially reduced 1:3 AuPd nanoparticles and co-reduced 1:3 AuPd nanoparticles. The disappearance of the surface plasmon peak at ~530 nm, which is characteristic for Au nanoparticles,[46] is consistent with observations seen by ourselves and others for the formation of Pd rich surfaces upon reduction

Scheme 1. Formation of Sequentially-Reduced AuPd Nanoparticles via the Reduction of K_2PdCl_4 onto the Surface of Au Nanoparticle Seeds in the Presence of Ascorbic Acid

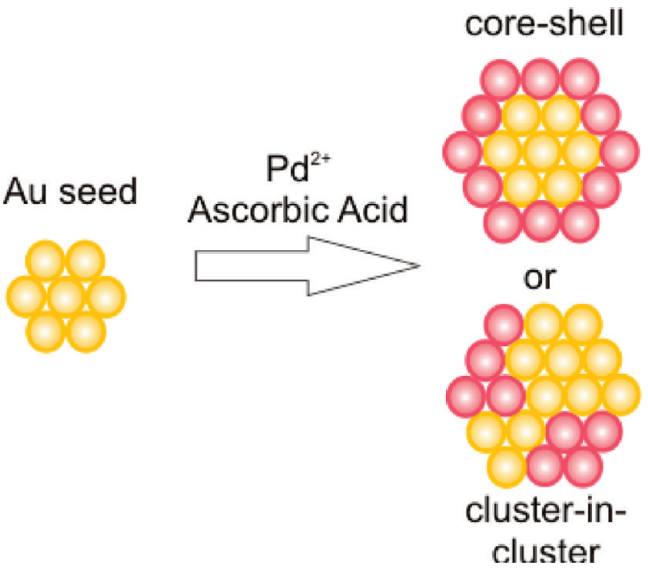

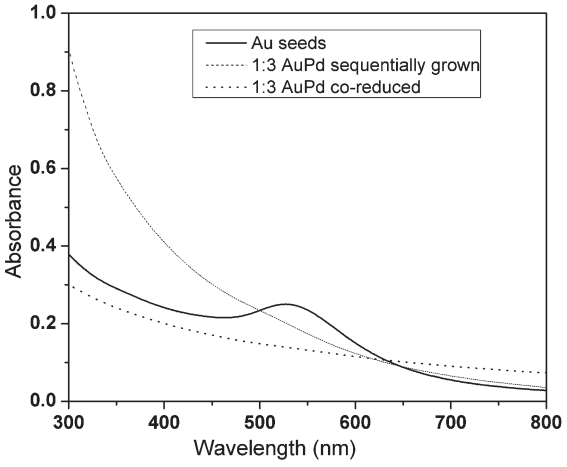

Figure 1. UV−vis spectra of PVP-stabilized Au nanoparticles, and sequentially reduced and co-reduced 1:3 AuPd nanoparticles.

of the Pd salts onto the Au seeds.[21,32] However it should be noted that while UV−vis data can suggest the formation of bimetallic nanoparticles, it must be complemented by other data, such as TEM and EXAFS data.

TEM images of the Au seed nanoparticles, sequentially grown 1:3 AuPd nanoparticles, and co-reduced 1:3 AuPd nanoparticles are shown in Figure 2. The average size of the PVP stabilized Au and AuPd nanoparticles were found to be 2.8 ± 0.7 nm and 4.2 ± 0.9 nm, respectively. The size increase is fairly consistent with the respective metal loadings of the core and shell, respectively according to eq 1 which is calculated to be 4.3 nm:[47]

$$D = D_{\text{core}}\left[1 + \frac{V_{\text{Pd}}[\text{Pd}]}{V_{\text{Au}}[\text{Au}]}\right]^{1/3} \quad (1)$$

where D_{core} is the diameter of the experimentally measured Au seed and V_{Au} and V_{Pd} and [Au] and [Pd] are the molar volumes

dx.doi.org/10.1021/cs200040a |ACS Catal. 2011, 1, 425–436

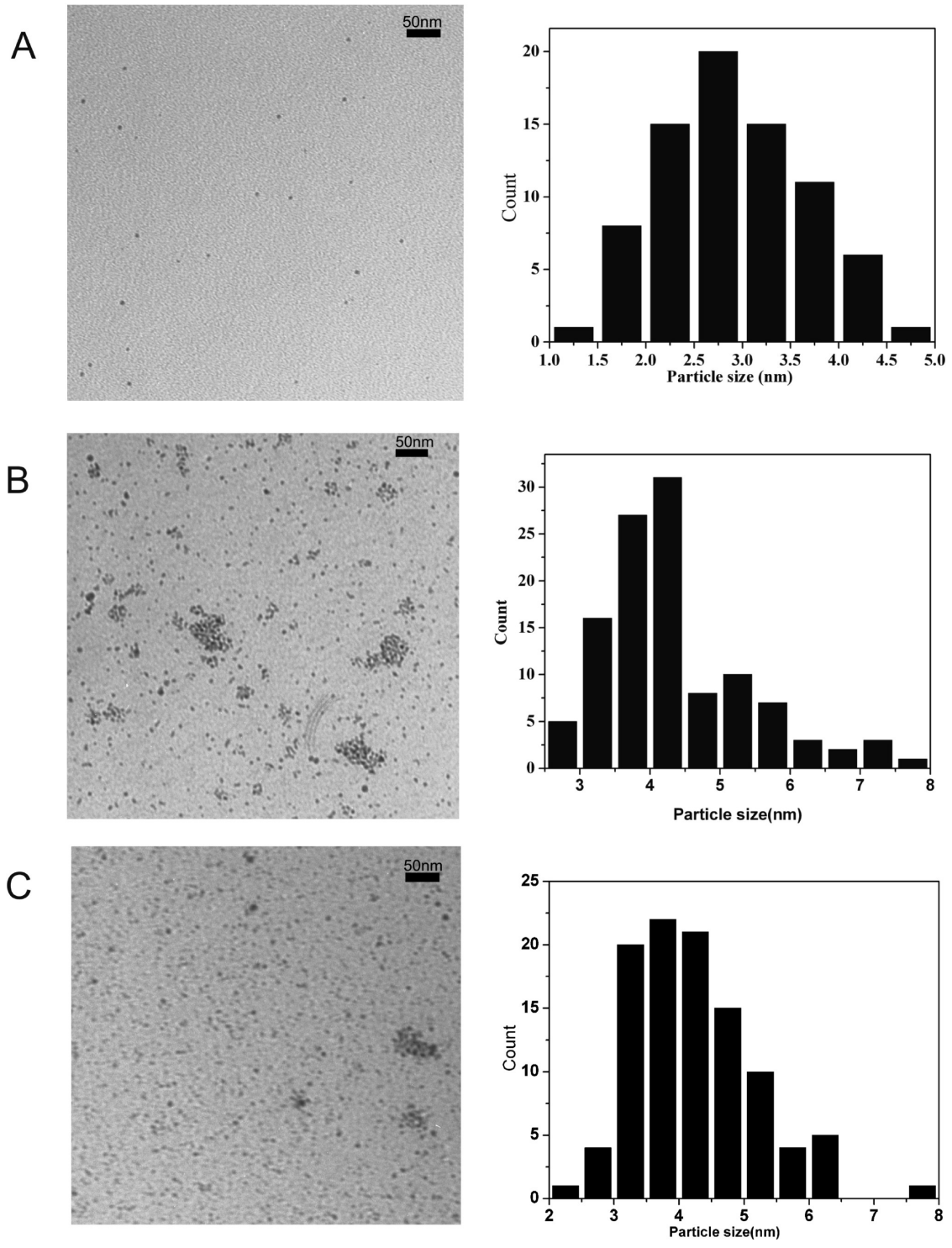

Figure 2. TEM images of PVP-stabilized (A) Au seeds and (B) sequentially reduced 1:3 AuPd nanoparticles and (C) co-reduced 1:3 AuPd nanoparticles and their respective particle size distributions.

and concentrations of Au and Pd, respectively. The increase in particle size and mild increase in the standard deviation of particle sizes is consistent with sequential core-shell growth and the absence of secondary nucleation of pure Pd nanoparticles. Figure 2C shows the TEM and particle size distribution of 1:3 AuPd co-reduced nanoparticles which have a similar particle size distribution of 3.9 ± 0.9 nm.

The UV−vis and TEM observations were supported by X-ray absorption studies. Figure 3A and 3B shows the Au L_{III}-edge and Pd K-edge EXAFS spectra in *k*-space for the pure Pd nanoparticles and sequentially reduced 1:3 and 1:1 AuPd nanoparticles; high quality data was collected over a *k*-range from 0 to 14. Several features in the spectra are quite interesting; the dampening of the amplitude of the signal in Figure 3B of the sequentially

dx.doi.org/10.1021/cs200040a |*ACS Catal.* 2011, 1, 425–436

grown 1:3 and 1:1 AuPd nanoparticles indicates significantly lower coordination numbers around Pd in the sequentially reduced particles (relative to pure Pd particles), whereas significant increases in the amplitude and thus coordination numbers around Au can be seen in Figure 3A upon sequential reduction of Pd onto the surface. In addition, no significant shift in the periodicity of the EXAFS wave is seen as compared to pure Pd nanoparticles, which contrasts with earlier work on AuPd alloys by both ourselves and others in which periodic changes in the periodicity of the EXAFS wave were seen because of changing bond distances as a result of AuPd mixing.[33,34] The absence of any shift in the oscillation peaks for the core-shell particles suggests that the extent of alloying between the two metals is very low.

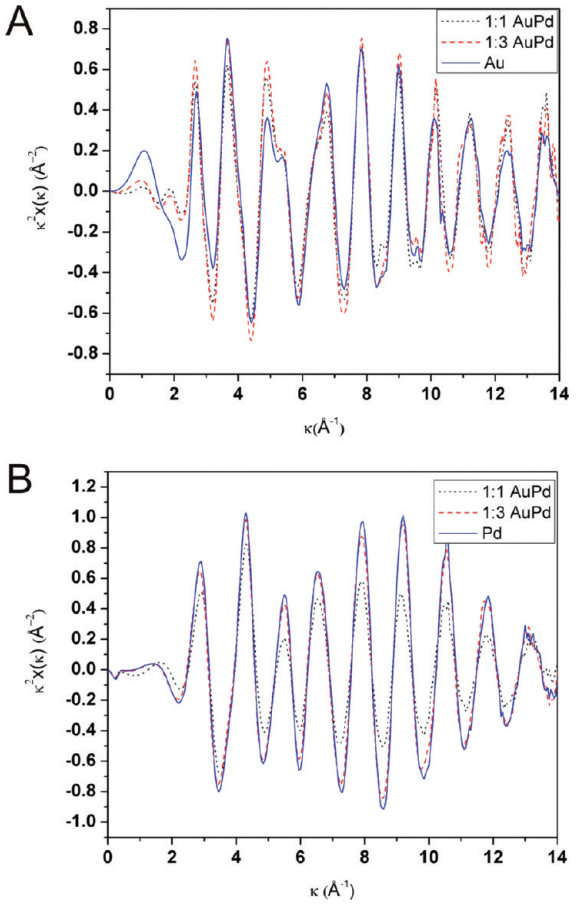

Figure 3. EXAFS spectra in *k*-space for pure metallic nanoparticles and sequentially reduced 1:3 and 1:1 AuPd nanoparticles. (A) Pd K-edge (B) Au-L_{III} edge.

Figure 4 shows the experimentally obtained EXAFS data with the single-shell theoretical fits for the pure Au and Pd nanoparticles as well as the sequentially reduced 1:3 AuPd nanoparticles. For the bimetallic nanoparticles, the Au and Pd EXAFS data of the same sample were simultaneously fit using the IFEFFIT software package.[41] High-quality fits have been obtained for most of the as synthesized metallic and bimetallic nanoparticles; the only exception is the case of the Pd edges in which some oxidation was apparent in the 1:1 sequentially reduced AuPd nanoparticles. The structural fit parameters for all the pure metallic and AuPd nanoparticles generated from the EXAFS fitting parameters are presented in Table 1. The low r-value shoulder on (particularly the 1:1 AuPd sample) is likely due to Pd oxidation and/or PVP coordination to the particles. For the bimetallic systems the total CNs were obtained from the summation of two coordination numbers as follows: $N_{Au\text{-}M} = N_{Au-Au} + N_{Au-Pd}$ and $N_{Pd\text{-}M} = N_{Pd-Pd} + N_{Pd-Au}$. The first shell coordination numbers (CNs) for pure gold and palladium nanoparticles, N_{Au-Au} and N_{Pd-Pd}, were found to be 10.0(1.4) and 9.9(0.5), respectively, which are lower than the bulk fcc CNs of 12. This is due to the significant fraction of atoms on the surface of the nanoparticles which have much lower CNs. The Au−Au bond distances in the pure Au particles is 2.82 Å, which is lower than the corresponding bulk value of 2.86 Å. This is consistent with the findings of others and is thought to be due to increased d-d interactions in small Au nanoparticles because of hybridization.[48] The $N_{Au\text{-}M}$ for 1:3 and 1:1 sequentially reduced AuPd particles are 11.9 and 10.4, respectively, while the $N_{Pd\text{-}M}$ are significantly lower at 10.5 and 8.8, respectively. This is a good indication of the presence of significantly Pd-rich surfaces and Au-rich cores within the particles,[35,49] though the fact that the Au CNs are consistently below 12 indicates that perfect core-shell structures are likely not formed, but rather cluster-in-cluster structures are formed (Scheme 1). Also of note is the fact that moderate levels of Pd oxidation on the surface are present, particularly in the AuPd 1:1 sample. Previous work in our group found that co-reduced AuPd nanoparticles have a near-alloy structure albeit with slightly higher Au loadings in the core and higher Pd loadings in the shell.[33]

To get additional information on the electronic effect and its correlation with the catalytic activity, the Au-L_{III} and Pd-L_{III} XANES

Table 1. EXAFS Fitting Parameters for All Nanoparticle Systems Studied

nanoparticle sample	shell	*N*	R_j(Å)	ΔE^o(eV)	σ^2(Å^2)	*R*-factor
pure Au	Au−Au	10.0(1.4)	2.82(0.01)	3.8 (1.0)	0.013(0.001)	0.016
pure Pd	Pd−Pd	9.9(0.5)	2.743(0.003)	−5.7(0.4)	0.0082(0.0004)	0.006
AuPd 1:3 sequential	Au−Au	8.7(1.6)	2.82(0.01)	3.7(0.9)	0.010(0.002)	0.005
	Au−Pd	3.2(1.0)	2.75(0.02)		0.012(0.004)	
	Pd−Pd	8.3(0.7)	2.744(0.005)	−5.5(0.6)	0.0073(0.0005)	
	Pd−Au	2.2(1.4)	2.76(0.02)		0.012(0.004)	
AuPd 1:1 sequential	Au−Au	8.3(1.5)	2.82(0.01)	3.7(0.8)	0.009(0.002)	0.014
	Au−Pd	2.1(0.9)	2.75(0.02)		0.008(0.003)	
	Pd−Pd	6.2(1.1)	2.73(0.01)	−4.2(0.9)	0.008(0.003)	
	Pd−Au	2.6(1.3)	2.75(0.02)		0.008(0.003)	
	Pd−O	1.4(0.6)	1.96(0.04)		0.010(0.003)	

dx.doi.org/10.1021/cs200040a |*ACS Catal.* 2011, 1, 425–436

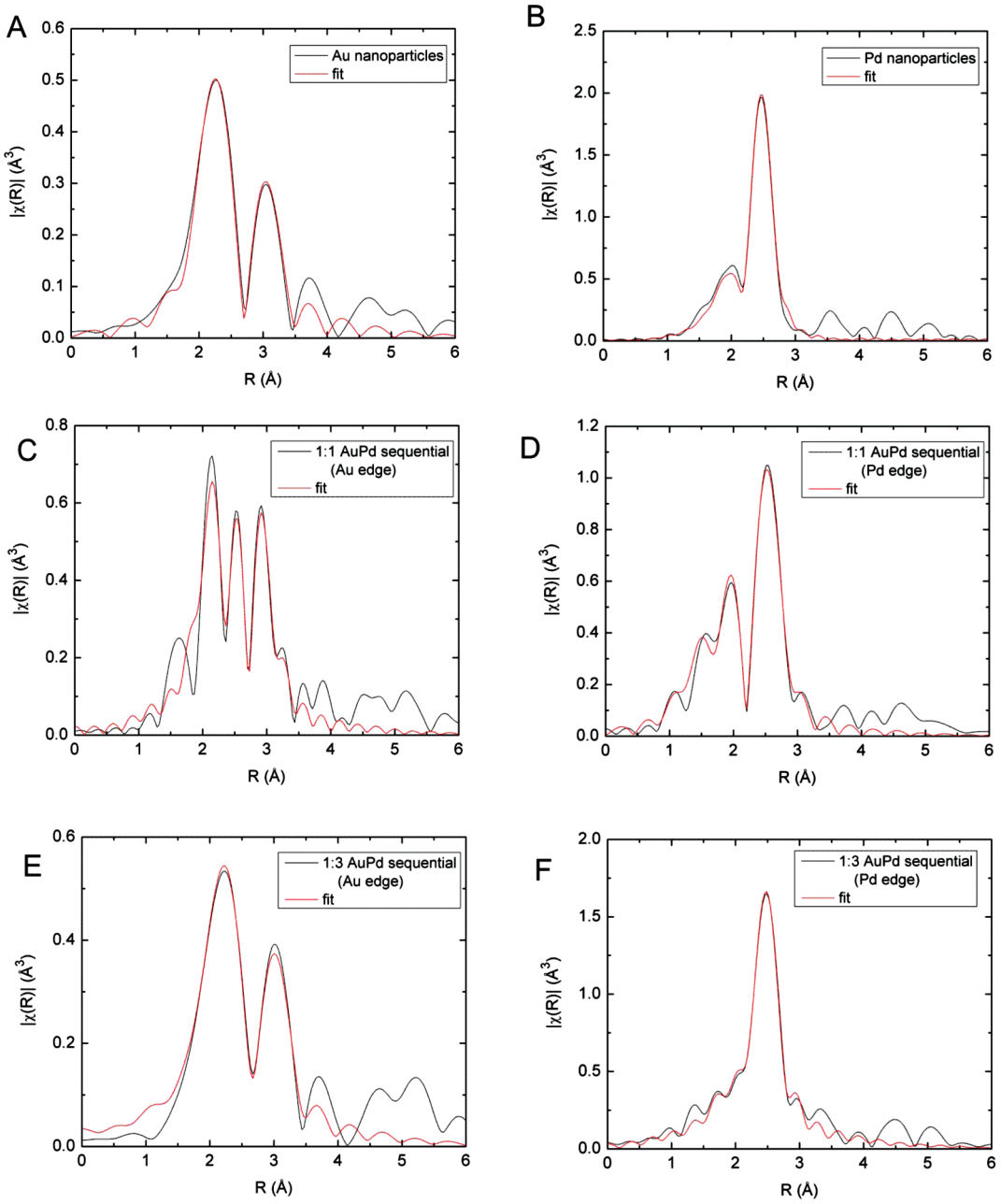

Figure 4. EXAFS single-shell fits in r-space for the as-synthesized nanoparticles at the Au-L_{III} and Pd K edges: (A) Au nanoparticles and (B) Pd nanoparticles; (C, D) sequentially reduced 1:1 AuPd nanoparticles as-synthesized, Au-edge and Pd-edge; (E, F) sequentially reduced 1:3 AuPd nanoparticles as synthesized, Au-edge and Pd-edge.

spectra for the AuPd nanoparticles were measured. The XANES spectra of the Au L_{III}-edge of as-synthesized Au, co-reduced 1:3 AuPd and sequentially reduced AuPd nanoparticles are shown in Figure 5A. The L_{III}-edge probes the transition of 2p electrons to the 5d orbitals; Au nanoparticles have a weaker white line shoulder (the first feature after the edge jump at 11925 eV) as compared to the bulk Au metal due to the lessening of s-p-d hybridization in such small Au nanoparticles as compared to bulk gold.[50] For all the bimetallic AuPd nanoparticles, a further decrease of the white line intensity occurs. This might possibly be due to electron transfer from Pd into 5d Au orbitals. The white line intensity of the co-reduced AuPd sample is much lower than that of core-shell nanoparticles indicating that alloying has significant effect on the occupancy of the Au-d band. Both ourselves and others have previously shown that increasing Pd content in AuPd alloys tends to increase the d-electron density leading to a decrease in the white line intensity.[33,34] For the sequentially reduced nanoparticles the intensity of the white line diminishes slightly as Pd content increases, as indicated by the higher white line intensity of the sequentially reduced 1:1 AuPd nanoparticles as compared to the 1:3 AuPd nanoparticles. One other important feature at the Au-L_{III} edge is the significant increase in the intensity of the second band (11935 eV) for the co-reduced nanoparticles as opposed to the sequentially reduced nanoparticles. This feature is caused by bimetallic distance effects in which interatomic redistribution of charge depends on interatomic distance.[51] The

dx.doi.org/10.1021/cs200040a |*ACS Catal.* 2011, 1, 425–436

reduction of this feature in the sequentially reduced system supports the lower level of mixing of the metals in the sequentially reduced particles. The Pd-L_{III} XANES spectra are shown in Figure 5B for the samples studied. A significant decrease in the d-occupancy as indicated by a more intense white line for the sequentially reduced samples as compared to the co-reduced sample was seen. However, we note that there are moderate levels

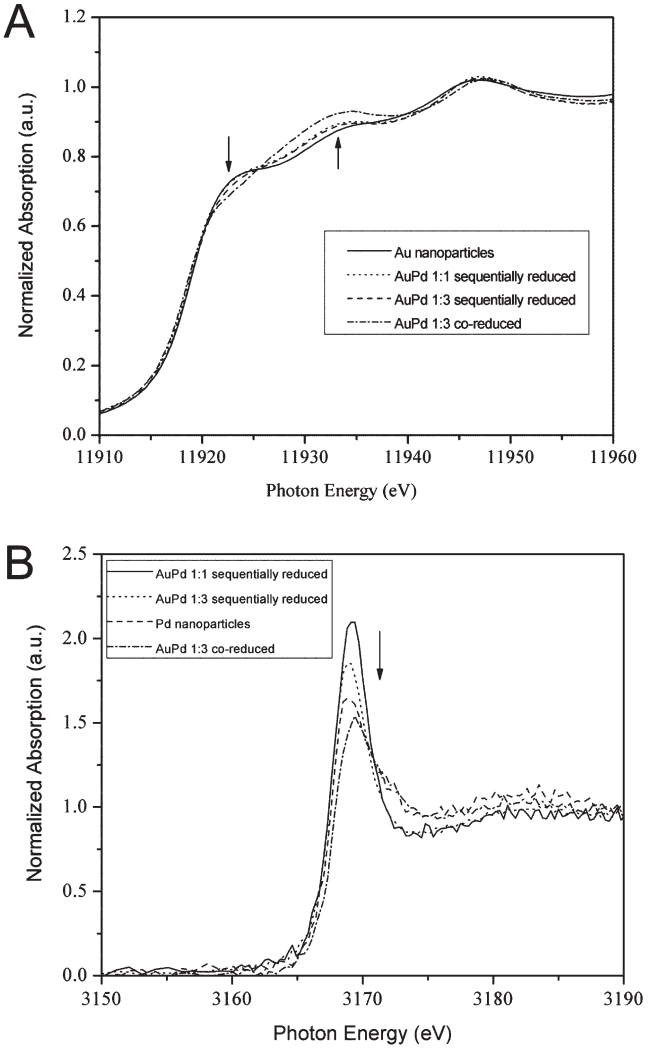

Figure 5. XANES spectra of as-synthesized nanoparticles, (A) Au-L_{III} edge, (B) Pd-L_{III} edge.

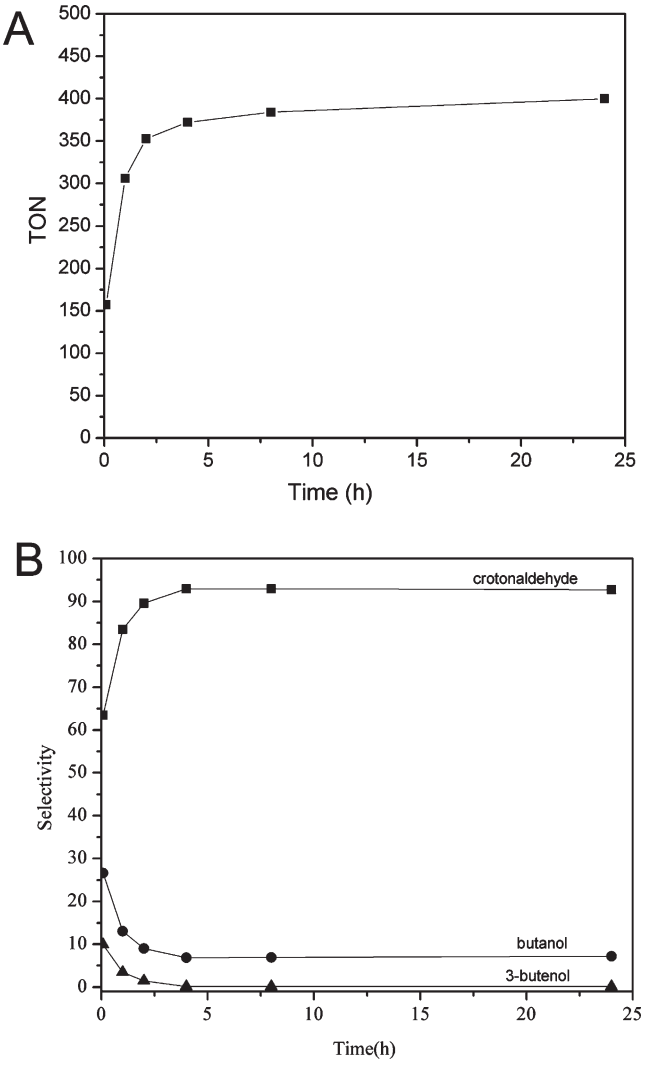

Figure 6. (A) Turnover number (TON) and (B) selectivity to crotonaldehyde for the oxidation of crotyl alcohol for sequentially reduced 1:3 AuPd nanoparticles.

Table 2. Summary of Catalytic Results for the Oxidation of Crotyl Alcohol[a]

				selectivity %		
entry	nanoparticle catalyst	TOF[b] (h^{-1})	conversion[c]	crotonaldehyde	1-butanol	3-butenol
1	Au	11	2.2	87.8	0.0	12.2
2	Pd	13	5.9	94.0	5.2	0.80
3	K_2PdCl_4	9	8.9	88.0	9.5	2.5
4	1:1 AuPd sequential	64	37.9	88.0	11.0	1.0
5	1:1.5 AuPd sequential	195	60.4	87.0	10.0	3.0
6	1:3 AuPd sequential	306	71.4	88.0	10.5	1.5
7	1:3 AuPd co-reduced	40	23.4	91.9	2.6	5.5
8	1:1 Au/Pd^{2+}	173	50.2	84.1	15.7	0.2
9	1:1.5 Au/Pd^{2+}	90	35.4	80.9	14.0	5.1
10	1:3 Au/Pd^{2+}	74	40.1	80.6	16.4	3.0
11	1:3 $PdPd^{2+}$	43	17.6	72.8	17.1	10.1
12	1:3 $PtPd^{2+}$	44	17.1	72.9	18.6	8.5

[a] Reaction conditions: All reactions are carried at 25 °C, the substrate/catalyst ratio is 520:1, 1.0×10^{-2} mol of crotyl alcohol added. [b] TOF was calculated for the first hour. [c] Conversion after 4 h.

dx.doi.org/10.1021/cs200040a |ACS Catal. 2011, 1, 425–436

Scheme 2. Mechanisms for the Selective Formation of Crotonaldehyde Using AuPd Nanoparticle Catalysts

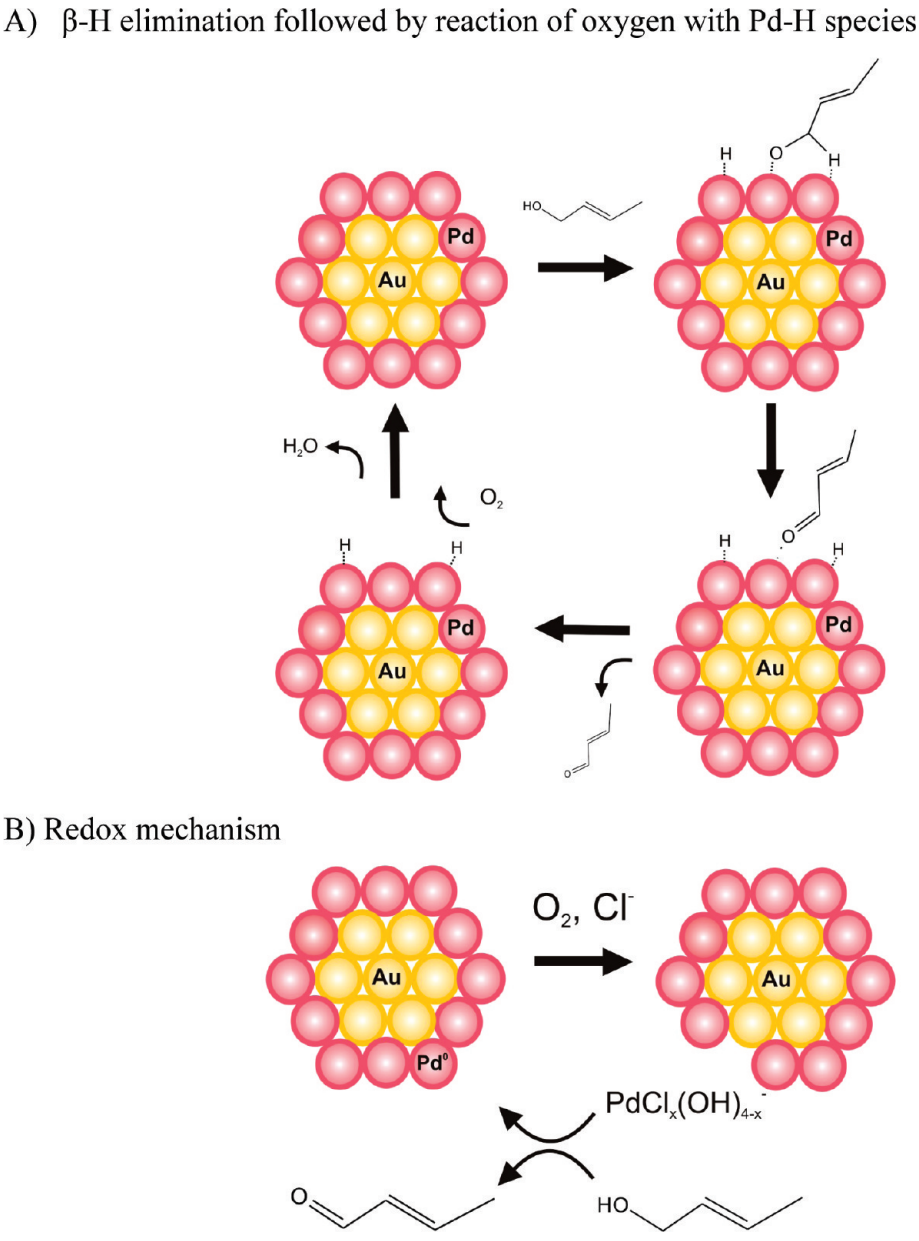

of surface oxidation in these samples (particularly the AuPd 1:1 sample), which will also lead to increases in the Pd-L_{III} white line intensity. The sequentially reduced nanoparticles have a more intense white line at the Pd-L_{III} edge as compared to the co-reduced samples; however, the Au-L_{III} data above suggests that the occupancy of the Au d-orbitals is highest in the co-reduced samples. This suggests that electronic interactions between metals in the particles is not as simple as d-charge transfer between Pd and Au atoms; indeed, others have noted that the occupancy of all the s, p, and d valence orbitals needs to be considered when examining electronic effects.[22]

The catalytic activity of the different nanoparticles toward the oxidation of crotyl alcohol was measured in aqueous solution and is summarized in Table 2 below. Our previous work showed that 1:3 AuPd co-reduced nanoparticles have a low conversion with a very poor selectivity to crotonaldehyde over the first hour at 62 °C, followed by an increase in selectivity over time.[20] In this work, reaction temperatures are 25 °C, and the base used in the earlier work (K_2CO_3) has been omitted while still retaining significant catalytic activity. Others have also shown that base-free alcohol oxidations can occur using Au and bimetallic catalysts.[7,14,15,21] A further advantage of the room temperature oxidation process is that decomposition of crotyl alcohol can occur over Pd surfaces at temperatures above room temperature to form CO and propene,[52] which can lead to lower turnover frequencies (TOFs) of the substrate and to the deactivation of the catalyst. Indeed, Lee et al. have recently shown that Pd-rich surface alloys are the optimal catalysts for minimal crotyl alcohol decomposition and maximum alcohol oxidation.[53] Pure Au and pure Pd nanoparticles have very low activity for crotyl alcohol

dx.doi.org/10.1021/cs200040a |ACS Catal. 2011, 1, 425–436

oxidation (entries 1 and 2, TOFs of 11 and 13 h^{-1}, respectively), and the co-reduced 1:3 AuPd nanoparticles have a TOF of 40 h^{-1} under the same conditions. However, sequentially reduced 1:1, 1:1.5, and 1:3 AuPd nanoparticles have significantly higher activities, with TOFs of 64, 195, and 306 h^{-1}, respectively, and selectivities for crotonaldehyde formation as high as 88%. Particle size effects should be negligible given the relatively similar sizes of the co-reduced and sequentially reduced 1:3 AuPd nanoparticles (above). The other products seen were the hydrogenation and isomerization products which can form in the presence of Pd−H species on surfaces.[20] We are not certain at this point why the 1:3 AuPd sequentially reduced system has the highest TON of the systems studied, but it likely is due to the near complete coverage of the Au cores by Pd shells and negligible oxidation of the surface Pd, whereas the 1:1 AuPd system may have lower catalytic activity because of surface oxidation. Turnover number (TON) and selectivity plots for 1:3 AuPd sequentially reduced nanoparticles are shown in Figure 6. As indicated in Figure 6A, the TON of this catalyst is very high over the first hour and reaches a maximum of 384 mols product/mol catalyst after 8 h. In addition, the selectivity of the reaction is low at the beginning of the reaction and increases significantly as the reaction proceeds. Hence, the bimetallic nanoparticles with Pd rich surfaces have high activity which indicates that even though Pd surface atoms are present in both the co-reduced and sequentially reduced AuPd nanoparticles, the Pd atoms on the surface of the core-shell particles are significantly more active, possibly because of d-charge depletion of these particles as seen in the XANES data above.

Reactions using a variety of other alcohol substrates (benzyl alcohol, 1,4-butanediol, 2-butanol) were also examined in these base-free, room temperature conditions. Very low conversions (5%) were seen at these conditions for benzyl alcohol, while no conversions were seen for 1,4 butanediol and 2-butanol. These results suggest that the mild conditions employed in this study may be somewhat unique for allylic alcohols. However the oxidation of primary and secondary alcohols by these core-shell AuPd catalysts can be achieved by mild increases in temperature and addition of base.[20]

Several mechanisms are possible for the selective formation of crotonaldehyde using the AuPd nanoparticle catalysts, as shown in Scheme 2. One mechanism which has been proposed involves β-H elimination followed by reaction of oxygen with Pd−H species.[8,20] Thus the role of oxygen in this mechanism is to clean the adsorbed H from the surface. Such mechanisms will likely give rise to low yields for the oxidation of allylic alcohols as the allyl groups can also act as H-atom scavengers to form hydrogenation products. Another possible mechanism is a redox mechanism in which the Pd surface is oxidized by oxygen, followed by the oxidation of alcohols by Pd(II) species and Pd(II) reduction back to Pd(0).[5,16] This would potentially establish a catalytic cycle in which the Pd(0) is regenerated and reoxidized. To further understand whether this mechanism might be at play, catalytic activity measurements using Pd(II) salts in the absence and presence of Au nanoparticles were carried out.

As indicated in Table 2, entries 7−10, although the K_2PdCl_4 salt is not, in of itself, particularly active for the oxidation of crotyl alcohol and shows a TOF of 9 h^{-1}, it does yield crotonaldehyde with 88% selectivity. In the presence of both K_2PdCl_4 and Au nanoparticles, significant conversions of crotyl alcohol were seen, with a TOF of 74 h^{-1} and 81% selectivity for crotonaldehyde using the 1:3 Au/Pd^{2+} catalyst system, as shown in Figure 7.

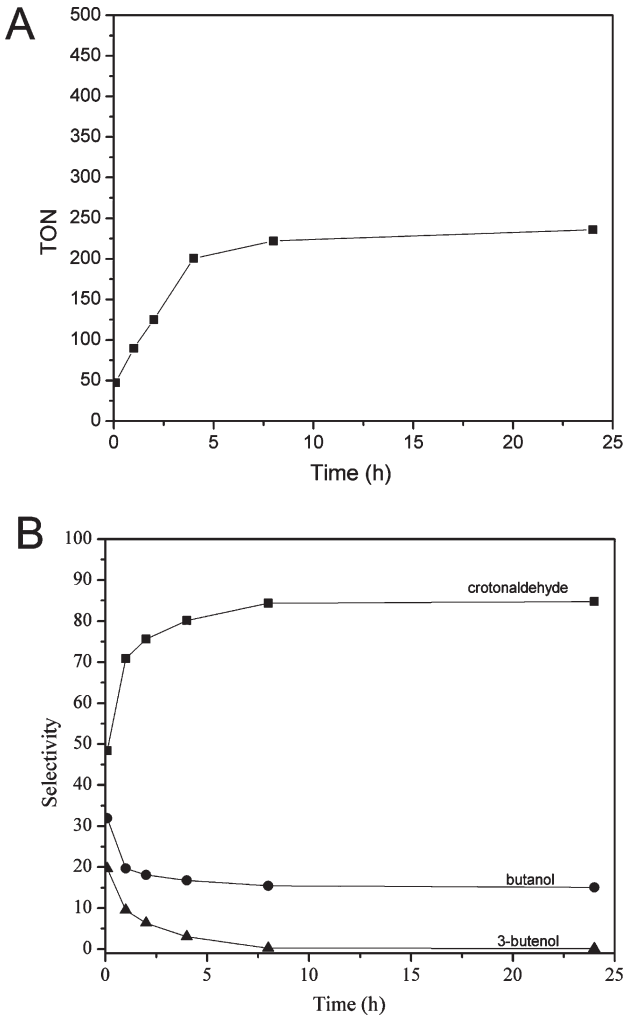

Figure 7. (A) Turnover number (TON) and (B) selectivity to crotonaldehyde for the oxidation of crotyl alcohol for Au nanoparticles with K_2PdCl_4.

TOFs of 90 and 173 h^{-1} were seen for Au/Pd^{2+} ratios of 1:1.5 and 1:1, respectively, with selectivities toward crotonaldehyde of 81 and 84%. These results support a Pd(II) mediated oxidation of crotyl alcohol with corresponding reduction of the Pd onto the Au nanoparticles which act as nucleation centers. This would then set up the cyclic redox mechanism as the Pd atoms on the nanoparticle surface can be reoxidized back to Pd(II) and participate in the reaction. We believe that activities are low for the pure K_2PdCl_4 system because of the lack of nucleation centers for Pd reduction. Control reactions using Pt and Pd nanoparticle seeds in the presence of K_2PdCl_4 showed moderate conversions and TONs, with slight drops in selectivity to crotonaldehyde (entry 11 and 12 of Table 2), albeit much lower than seen for Au nanoparticles in the presence of K_2PdCl_4. This indicates that the Au, which is more electronegative (Au electronegativity: 2.54, Pd: 2.20; Pt: 2.28), enhances the activity of the reaction via decreasing the d-electron density of the surface Pd, and thus making it more easily oxidized. If this mechanism is indeed occurring, then in situ growth of AuPd core-shell nanoparticles might be expected during the course of the reaction.

dx.doi.org/10.1021/cs200040a |ACS Catal. 2011, 1, 425–436

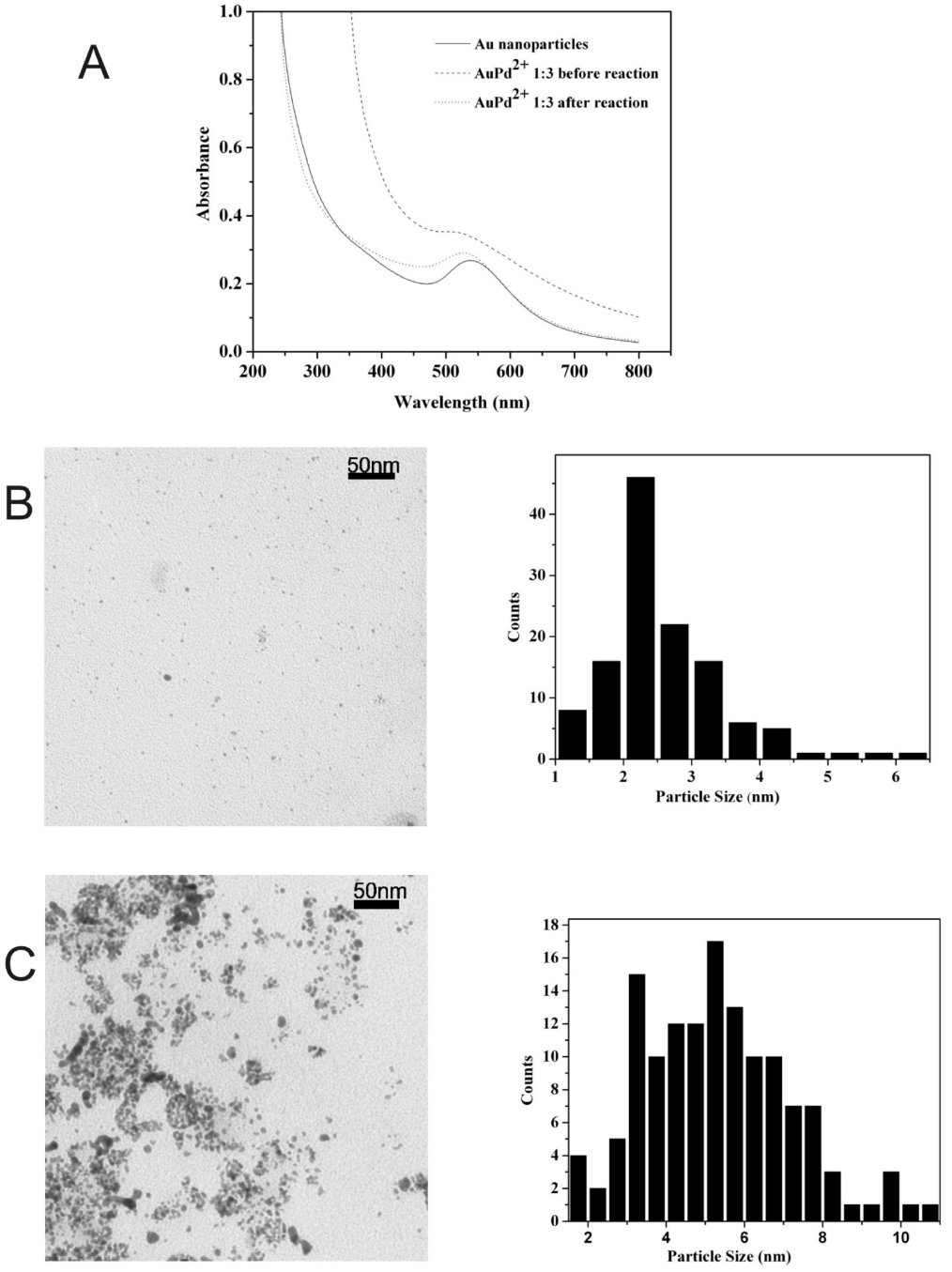

Figure 8. (A) UV−vis spectra and TEM images of Au nanoparticles in the presence of K_2PdCl_4, (B) before reaction and (C) after reaction, and their corresponding particle size distributions.

Indeed, as shown in Figure 8, the formation of Pd shells on the surface of the Au nanoparticles is supported by the UV−vis spectra (Figure 8A) which indicates a dampening of the surface plasmon band of the Au/Pd^{2+} mixture after the catalytic reaction suggesting the formation of Pd shells on the particles as the reaction progresses. Furthermore, from TEM measurements (Figure 8B and 8C), the average nanoparticle size for the 1:3 Au/Pd^{2+} system was 2.6 ± 0.6 nm before the catalytic reaction and 5.2 ± 2.2 nm afterward, confirming significant growth of the particle size during the reaction. No similar changes were seen for pure Au nanoparticles or pure K_2PdCl_4 salts. The data strongly supports the redox mechanism for the core-shell nanoparticles in which Pd oxidation and re-reduction occurs; however, we note that we cannot completely rule out the β-H elimination mechanism, which is likely occurring to some extent as well, as evidenced by the low levels of both hydrogenation and isomerization products. We note a recent paper by Prati and co-workers which also lends tremendous support to a redox mechanism, as they documented that bimetallic AuPd nanoparticles are the active catalyst despite starting with a system consisting of monometallic nanoparticles.[54] One detail that is still under investigation is whether this redox mechanism is a homogeneous and/or heterogeneous

dx.doi.org/10.1021/cs200040a |*ACS Catal.* 2011, 1, 425–436

catalytic process, that is, whether the active Pd(II) species for alcohol oxidation are on the surface of the particle or in the solution. Such questions of homogeneous versus heterogeneous catalytic processes using nanoparticle catalyst systems have been identified in other systems as well.[55]

CONCLUSIONS

We have synthesized PVP stabilized bimetallic AuPd nanoparticle catalysts using co-reduction and sequential reduction routes. Their structural and electronic properties were investigated using UV−vis, TEM, EXAFS, and XANES. The structural investigations suggest that sequentially reduced particles have significantly Pd-rich surfaces and Au-rich cores. Furthermore, a significant decrease in the white line intensity of the Pd-L_{III} XANES spectra for the sequentially reduced system indicates that Pd on the surface of such particles shows significant d-charge depletion. The sequentially reduced nanoparticles with Pd-rich surfaces were examined as catalysts for the room-temperature aerobic oxidation of crotyl alcohol and showed significantly enhanced activities and high selectivity to crotonaldehyde. For example, for the sequentially reduced 1:3 AuPd system, a TOF of 306 h^{-1} was seen with a selectivity to crotonaldehyde of 88%, which was significantly higher than the TOFs of co-reduced 1:3 AuPd (40 h^{-1}), pure Pd (13 h^{-1}) and Au (12 h^{-1}) nanoparticles. UV−vis and TEM measurements before and after the reaction together with catalytic activity measurements using K_2PdCl_4 in the absence and presence of Au nanoparticles indicate the system is catalytically active with both species present. This suggests a mechanism involving a redox cycle of Pd(II) to Pd(0) reduction and reoxidation with in situ formation of core-shell nanoparticles. However, we note that we cannot completely rule out the β-H elimination mechanism, which is likely occurring to some extent as well.

AUTHOR INFORMATION

Corresponding Author

*E-mail: robert.scott@usask.ca. Phone: 306-966-2017. Fax: 306-966-4730.

Funding Sources

The authors would like to thank NSERC and the University of Saskatchewan for funding. Research described in this paper was performed at the Canadian Light Source, which is supported by the Natural Sciences and Engineering Research Council of Canada, the National Research Council Canada, the Canadian Institutes of Health Research, the Province of Saskatchewan, Western Economic Diversification Canada, and the University of Saskatchewan.

ACKNOWLEDGMENT

The authors would like to thank Dr. Ning Chen and Yongfeng Hu at the Canadian Light Source (CLS) for the assistance with EXAFS and XANES measurements, and Michael Gaultois for assistance with the cover art.

REFERENCES

(1) Abad, A.; Almela, C.; Corma, A.; Garcia, H. *Tetrahedron* **2006**, *62*, 6666–6672.
(2) Zaw, K.; Lautens, M.; Henry, P. M. *Organometallics* **1983**, *2*, 197–199.
(3) Lee, D. G.; Spitzer, U. A. *J. Org. Chem.* **1970**, *35*, 3589–3590.
(4) Prabhakaran, P. V.; Venkatachalam, S.; Ninan, K. N. *Eur. Polym. J.* **1999**, *35*, 1743–1746.
(5) Muzart, J. *Tetrahedron* **2003**, *59*, 5789–5816.
(6) Prati, L.; Rossi, M. *J. Catal.* **1998**, *176*, 552–560.
(7) Enache, D. I.; Knight, D. W.; Hutchings, G. J. *Catal. Lett.* **2005**, *103*, 43–52.
(8) Tsunoyama, H.; Sakurai, H.; Negishi, Y.; Tsukuda, T. *J. Am. Chem. Soc.* **2005**, *127*, 9374–9375.
(9) Abad, A.; Almela, C.; Corma, A.; Garcia, H. *Chem. Commun.* **2006**, 3178–3180.
(10) Tsunoyama, H.; Tsukuda, T.; Sakurai, H. *Chem. Lett.* **2007**, *36*, 212–213.
(11) Li, H.; Guan, B.; Wang, W.; Xing, D.; Fang, Z.; Wan, X.; Yang, L.; Shi, Z. *Tetrahedron* **2007**, *63*, 8430–8434.
(12) Hu, J.; Chen, L.; Zhu, K.; Suchopar, A.; Richards, R. *Catal. Today* **2007**, *122*, 277–283.
(13) Tsunoyama, H.; Ichikuni, N.; Sakurai, H.; Tsukuda, T. *J. Am. Chem. Soc.* **2009**, *131*, 7086–7093.
(14) Casanova, O.; Iborra, S.; Corma, A. *J. Catal.* **2009**, *265*, 109–116.
(15) Liu, H.; Liu, Y.; Li, Y.; Tang, Z.; Jiang, H. *J. Phys. Chem. C* **2010**, *114*, 13362–13369.
(16) Mifsud, M.; Parkhomenko, K. V.; Arends, I. W. C. E; Sheldon, R. A. *Tetrahedron* **2010**, *66*, 1040–1044.
(17) Ma, Z.; Yang, H.; Qin, Y.; Hao, Y.; Li, G. *J. Mol. Catal. A: Chem.* **2010**, *331*, 78–85.
(18) Enache, D. I.; Edwards, J. K.; Landon, P.; Solsona-Espriu, B.; Carley, A. F.; Herzing, A. A.; Watanabe, M.; Kiely, C. J.; Knight, D. W.; Hutchings, G. J. *Science* **2006**, *311*, 362–365.
(19) Dimitratos, N.; Lopez-Sanchez, J. A.; Lennon, D.; Porta, F.; Prati, L.; Villa, A. *Catal. Lett.* **2006**, *108*, 147–153.
(20) Hou, W.; Dehm, N. A.; Scott, R. W. J. *J. Catal.* **2008**, *253*, 22–27.
(21) Villa, A.; Janjic, N.; Spontoni, P.; Wang, D.; Su, D. S.; Prati, L. *Appl. Catal., A* **2009**, *364*, 221–228.
(22) Marx, S.; Baiker, A. *J. Phys. Chem. C.* **2009**, *113*, 6191–6201.
(23) Frank, A. J.; Rawski, J.; Maly, K. E.; Kitaev, V. *Green Chem.* **2010**, *12*, 1615–1622.
(24) Chen, Y.; Lim, H.; Tang, Q.; Gao, Y.; Sun, T.; Yan, Q.; Yang, Y. *Appl. Catal., A* **2010**, *380*, 55–65.
(25) Haruta, M. *Catal. Today* **1997**, *36*, 153–166.
(26) Lai, X.; Goodman, D. W. *J. Mol. Catal. A: Chem.* **2000**, *162*, 33–50.
(27) Bianchi, C. L.; Canton, P.; Dimitratos, N.; Porta, F.; Prati, L. *Catal. Today* **2005**, *102−103*, 203–212.
(28) Ketchie, W. C.; Fang, Y. L.; Wong, M. S.; Murayama, M.; Davis, R. J. *J. Catal.* **2007**, *250*, 94–101.
(29) Han, Y. F.; Zhong, Z.; Ramesh, K.; Chen, F.; Chen, L.; White, T.; Tay, Q.; Yaakub, S. N.; Wang, Z. *J. Phys. Chem. C* **2007**, *111*, 8410–8413.
(30) Edwards, J. K.; Solsona, B.; Ntainjua, N. E.; Carley, A. F.; Herzing, A. A.; Kiely, C. J.; Hutchings, G. J. *Science* **2009**, *323*, 1037–1041.
(31) Toshima, N.; Yonezawa, T. *New. J. Chem.* **1998**, *22*, 1179–1201.
(32) Scott, R. W. J.; Wilson, O. M.; Oh, S. K.; Kenik, E. A.; Crooks, R. M. *J. Am. Chem. Soc.* **2004**, *126*, 15583–15591.
(33) Dash, P.; Bond, T.; Fowler, C.; Hou, W.; Coombs, N.; Scott, R. W. J. *J. Phys. Chem. C.* **2009**, *113*, 12719–12730.
(34) Liu, F.; Wechsler, D.; Zhang, P. *Chem. Phys. Lett.* **2008**, *461*, 254–259.
(35) Knecht, M. R.; Weir, M. G.; Frenkel, A. I.; Crooks, R. M. *Chem. Mater.* **2008**, *20*, 1019–1028.
(36) Harada, M.; Asakura, K.; Toshima, N. *J. Phys. Chem. C* **1993**, *97*, 5103–5114.
(37) Mejia-Rosales, S. J.; Fernandez-Navarro, C.; Perez-Tijerina, E.; Blom, D. A.; Allard, L. F.; Jose-Yacaman, M. *J. Phys. Chem. C* **2007**, *111*, 1256–1260.
(38) Chen, C.-H.; Sarma, L. S.; Chen, J.-M.; Shih, S.-C.; Wang, G.-R.; Liu, D.-G.; Tang, M.-T.; Lee, J.-F.; Hwang, B.-J. *ACS Nano* **2007**, *1*, 114–125.

(39) Lu, L.; Wang, H.; Xi, S.; Zhang, H. *J. Mater. Chem.* **2002**, *12*, 156–158.
(40) Breining, M.; Chen, M. H.; Ice, G. E.; Parente, F.; Crasemann, B.; Brown, G. S. *Phys. Rev. A* **1980**, *22*, 520–528.
(41) Newville, M. *J. Synchrotron Radiat.* **2001**, *8*, 322–324.
(42) Newville, M.; Ravel, B.; Haskel, D.; Rehr, J. J.; Stern, E. A.; Yacoby, Y. *Phys. B.* **1995**, *208*, 154–156.
(43) Fang, Y.-L.; Miller, J. T.; Guo, N.; Heck, K. N.; Alvarez, P. J. J.; Wong, M. S. *Catal. Today* **2011**, *160*, 96–102.
(44) Maeland, A.; Flanagan, T. B. *Can. J. Phys.* **1964**, *42*, 2364–2366.
(45) Ott, L. S.; Hornstein, B. J.; Finke, R. G. *Langmuir* **2006**, *22*, 9357–9367.
(46) Dash, P.; Dehm, N. A.; Scott, R. W. J. *J. Mol. Catal. A: Chem.* **2008**, *286*, 114–119.
(47) Hodak, J. H.; Henglein, A.; Giersig, M.; Hartland, G. V. *J. Phys. Chem. B* **2000**, *104*, 11708–11718.
(48) Bus, E.; van Bokhoven, J. A. *J. Phys. Chem. C* **2007**, *111*, 9761–9768.
(49) Oxford, S. M.; Lee, P. L.; Chupas, P. J.; Chapman, K. W.; Kung, M. C.; Kung, H. H. *J. Phys. Chem. C* **2010**, *114*, 17085–17091.
(50) van Bokhoven, J. A.; Miller, J. T. *J. Phys. Chem. C* **2007**, *111*, 9245–9249.
(51) Pedersen, M. O.; Helveg, S.; Ruban, A.; Stensgaard, I.; Laegsgaard, E.; Norskov, J. K.; Besenbacher, F. *Surf. Sci.* **1999**, *426*, 395–409.
(52) Lee, A. F.; Chang, Z.; Ellis, P.; Hackett, S. F. J.; Wilson, K. *J. Phys. Chem. C* **2007**, *111*, 18844–18847.
(53) Lee, A. F.; Hackett, S. F. J.; Hutchings, G. J.; Lizzit, S.; Naughton, J.; Wilson, K. *Catal. Today* **2009**, *145*, 251–257.
(54) Wang, D.; Villa, A.; Spontoni, P.; Su, D. S.; Prati, L. *Chem.—Eur. J.* **2010**, *16*, 10007–10013.
(55) Astruc, D.; Lu, F.; Aranzaes, J. R. *Angew. Chem., Int. Ed.* **2005**, *44*, 7852–7872.

NOTE ADDED AFTER ASAP PUBLICATION

After this paper was published online March 23, 2011, a correction was made to the Acknowledgment. The revised version was published April 19, 2011.